Chemical Physics Letters 476 (2009) 125–134

Contents lists available at ScienceDirect

Chemical Physics Letters

journal homepage: www.elsevier.com/locate/cplett

FRONTIERS ARTICLE

Adsorbates on graphene: Impurity states and electron scattering

T.O. Wehling [a,*], M.I. Katsnelson [b], A.I. Lichtenstein [a]

[a] I. Institut für Theoretische Physik, Universität Hamburg, Jungiusstraße 9, D-20355 Hamburg, Germany
[b] Institute for Molecules and Materials, Radboud University of Nijmegen, Heijendaalseweg 135, 6525 AJ Nijmegen, The Netherlands

ARTICLE INFO

Article history:
Received 29 May 2009
In final form 3 June 2009
Available online 6 June 2009

ABSTRACT

In this review, we discuss adsorbate effects on the electronic properties of graphene. Firstly, different interaction mechanisms of impurities with graphene are introduced in terms of simple models. We discuss the requirements for impurity states in the vicinity of the Fermi level and compare graphene to normal metals and semiconductors. With this background, we consider realistic adsorbates based on density functional theory. Open-shell and inert impurities exhibit very different interaction mechanisms with graphene. The former interact directly with graphene, strongly hybridize or become charged, whereas inert impurities usually physisorb and substrate mediated doping effects become very important.

1. Introduction

Carbon is one of the most outstanding elements in the periodic table: it forms stable 4-fold coordinated sp^3 hybrids like diamond, 2-fold coordinated sp hybrids like acetylene, as well as stable 3-fold coordinated sp^2 hybrids like benzene or graphene. The latter allotrope, made up by carbon atoms arranged in a two dimensional (2-d) honeycomb lattice, is a building block for three dimensional graphite, 'one dimensional' carbon nanotubes and 'zero dimensional' fullerenes. These derived materials were discovered before graphene but their behavior already pointed towards one of graphene's most remarkable properties: the carbon atoms in graphene 'are completely naked from above and below' but they are 'largely immune to further bonding', as stated by Smalley in his 1996 Nobel lecture [1].

The first experimental realization of graphene [2] about 8 years later initiated enormous interest in this material. In addition to being the first truly two dimensional material and being surprisingly inert, graphene became famous for its remarkable electronic properties [3–5]. Its 2-d crystal structure leads to electrons behaving like massless fermions with the speed of light being replaced by the Fermi velocity $v \approx 10^6$ m/s. Electrons in graphene show extraordinarily high charge carrier mobility μ [2,6,7] which – in combination with the very high Fermi velocity – makes micron mean free paths routinely achievable. These properties are particularly prospective for applications like ultra-high frequency transistors, gas sensors or as transparent flexible electrode material for display technology. Indeed, as large scale high quality graphene samples grown by a technique called chemical vapor deposition [8] are becoming available, graphene applications are appearing more and more realistic. It is even discussed whether graphene could replace silicon in electronics industry. This question is still open, as opening a band gap in graphene without destroying the high electron mobility remains to be archived.

Applications exploiting graphene's unique electronic properties require us to understand impurity effects in this material. First, residual impurities from the production process are inevitable sources of electron scattering and they might limit electron transport in graphene. Indeed, the mechanism limiting the electron mobility in graphene is still under debate. Charged impurities [9–11], resonant impurities [12,13] and frozen ripples [14] are among the candidates, with the former two being addressed in this review.

More than just being undesirable obstacles, impurities provide a powerful tool for controlling and examining the electronic properties of solid state materials. Graphene is a model system for studying relativistic quantum physics in condensed matter [15,16] and impurity states in this material are directly related to scattering of relativistic quasiparticles [12,17–21]. Peculiarities of impurity scattering in graphene will be worked out in this review. Present graphene samples can be doped both by gate voltages [2] and chemically [2,22,23]. Thus, impurity states can be controlled to achieve desired material properties, and graphene functions as chemical sensor with respect to its dopants. The microscopic mechanisms responsible for doping and adsorbate sensitivity of graphene will be explained herein.

In the following section, we briefly introduce the Green function formalism which allows us to address the local electronic properties of graphene in presence of impurities. A comparison of strongly schematized graphene with a model semiconductor and a model metal is given in this framework (Section 2.1). We find that certain types of impurities create resonances in the vicinity of the Dirac point and discuss the nature of these 'midgap states' in Section 2.2. Section 3 is devoted to realistic density functional theory-based studies of impurity effects in graphene. We show

* Corresponding author.
E-mail address: twehling@physnet.uni-hamburg.de (T.O. Wehling).

0009-2614/$ - see front matter © 2009 Elsevier B.V. All rights reserved.
doi:10.1016/j.cplett.2009.06.005

that there are two distinct classes of impurities, open-shell impurities (Section 3.1) and inert impurities (Section 3.2). The former interact directly with graphene and become charged or strongly hybridized. The latter interact weakly with graphene, but may still lead to doping by mediating interactions between graphene and its substrate. Section 4 summarizes the main results and gives an outlook to future developments.

2. Models of impurities in graphene

To study impurity effects in graphene it is insightful to follow the way from simple, but crude, to realistic, but more complicated, models. We first compare impurities in a metal with rectangular density of states and a semiconductor with gapped DOS to the intermediate case of a graphene-like host with 'V'-shape density of states. These models can be treated fully analytically and allow us to understand the similarities and differences of graphene, normal semiconductors, and simple metals. In the next step, we consider impurities in a tight-binding model of graphene, which allows us to include atomistic details of the impurity; finally, we discuss the effect of impurities bringing along additional orbitals, which hybridize with the graphene bands.

2.1. Hosts with schematized electronic structure

A simple model of a metal, a semiconductor and graphene is obtained from an unperturbed Hamiltonian

$$\hat{H} = \sum_k \epsilon_k c_k^\dagger c_k, \tag{1}$$

where c_k are Fermi operators of electrons labelled by the quantum number $k = (\vec{k}, \nu)$, which contains the crystal momentum $\vec{k}$ and the band index ν. The spin-index is omitted for simplicity. ϵ_k is the energy of the electron in the state k and the Fermi energy is defined to be $E_f = 0$.

A short range spherically symmetric impurity can be imagined as a δ-function potential $V(x) = V\delta(x)$ and reads as $\hat{V} = V\sum_{k,k'} c_k^\dagger c_{k'}$ in this model.

The associated impurity effect on the electronic properties of the system can be obtained using Green function techniques: the unperturbed Green function is given by $\hat{G}^0(E) = (E - \hat{H} + i\delta)^{-1}$ and has matrix elements $G^0_{k,k'}(E) = \delta_{k,k'}\frac{1}{E-\epsilon_k+i\delta}$. The full Green function

$$\hat{G}(E) = (E - \hat{H} - \hat{V} + i\delta)^{-1} \tag{2}$$

is then

$$\hat{G}(E) = \hat{G}^0(E) + \hat{G}^0(E)\hat{T}(E)\hat{G}^0(E), \tag{3}$$

where the T-matrix is

$$\hat{T}(E) = \left(1 - \hat{V}\hat{G}^0(E)\right)^{-1}\hat{V}. \tag{4}$$

All single particle observables can be calculated from this Green function. Of particular interest is the local density of states, N (LDOS), in the vicinity of the impurity which is, e.g., probed by scanning tunneling spectroscopy. At any point $\vec{r}$, the LDOS is given by $N(\vec{r}, E) = -\frac{1}{\pi}\mathrm{Im}G(\vec{r}, \vec{r}, E)$, where $G(\vec{r}, \vec{r}, E)$ is the real space representation of the Green function $\hat{G}(E)$:

$$G(\vec{r}, \vec{r}, E) = \sum_{k,k'} G_{k,k'}(E) e^{i(\vec{k}-\vec{k}')\cdot\vec{r}}. \tag{5}$$

As the unperturbed system is homogeneous and its real space Green function is independent of $\vec{r}$, we can define the local unperturbed Green function $g_0(E) = G^0(\vec{r}, \vec{r}, E) = \sum_k \frac{1}{E-\epsilon_k+i\delta}$. Using the Cauchy principal value, $\mathscr{P}$, yields

$$g_0(E) = \mathscr{P}\sum_k \frac{1}{E-\epsilon_k} - i\pi N_0(E), \tag{6}$$

where $N_0(E) = \sum_k \delta(E-\epsilon_k)$ is the unperturbed local density of states, and consequently

$$\mathrm{Re}\, g_0(E) = \mathscr{P}\int_{-\infty}^{\infty} \frac{N_0(E')}{(E-E')}\mathrm{d}E'. \tag{7}$$

Specifying the unperturbed LDOS suffices to determine the local unperturbed Green function. As the matrix elements of the localized perturbation $\langle k|\hat{V}|k'\rangle = V$ considered here are independent of k and k', Eq. (4) simplifies to $\langle k|\hat{T}(E)|k'\rangle = T(E)$ with

$$T(E) = (1 - Vg_0(E))^{-1}V. \tag{8}$$

This toolkit will be now used to compare impurity resonances in different model materials:

- a metal with rectangular and symmetric DOS with respect to the Fermi level $N_0^{\mathrm{m}}(E) = \frac{1}{2D}\cdot\Theta(D-|E|)$ and resulting Green function $g_0^{\mathrm{m}}(E) = \frac{1}{2D}\ln|\frac{D+E}{D-E}| - i\pi N_0^{\mathrm{m}}(E)$;
- a semiconductor with gap Δ in the DOS $N_0^{\mathrm{s}}(E) = \frac{1}{2D}\cdot(\Theta(D+\Delta-|E|) - \Theta(\Delta-|E|))$ and $g_0^{\mathrm{s}}(E) = \frac{1}{2D}\ln|\frac{(D+\Delta+E)(\Delta-E)}{(D+\Delta-E)(\Delta+E)}| - i\pi N_0^{\mathrm{s}}(E)$;
- graphene with DOS $N_0^{\mathrm{g}}(E) = \frac{|E|}{D^2}\cdot\Theta(D-|E|)$ and $g_0^{\mathrm{g}}(E) = \frac{E}{D^2}\ln|\frac{E^2}{D^2-E^2}| - i\pi N_0^{\mathrm{g}}(E)$.

These unperturbed Green functions are depicted in Fig. 1. Eq. (3) shows that poles of the T-matrix cause impurity resonances, which occur according to Eq. (8) if

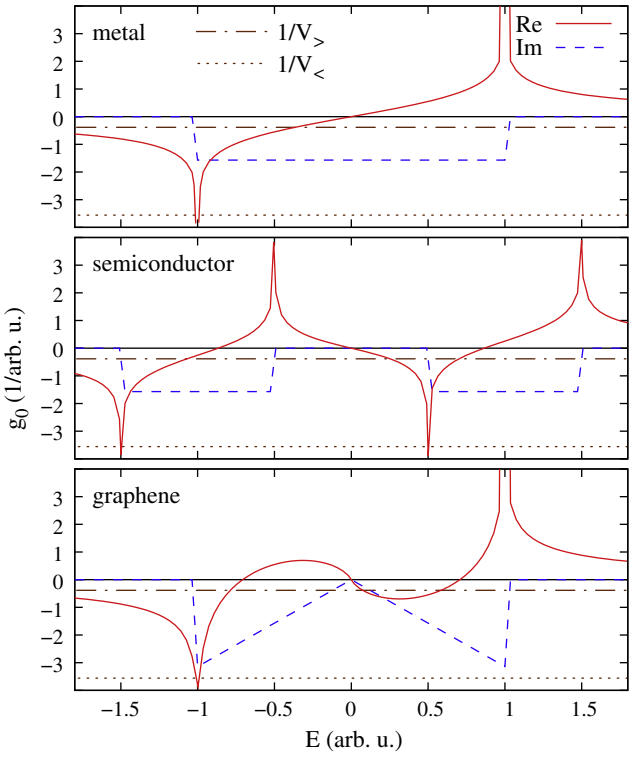

Fig. 1. Unperturbed model Green functions for a metal g_0^{m}, a semiconductor g_0^{s}, and a graphene g_0^{g}. (Here, the bandwidth parameter is $D = 1$ and the semiconductor's gap is $\Delta = \frac{1}{2}$). Real and imaginary parts are shown by solid and dashed lines, respectively. The real parts exhibit logarithmic divergences at band edges and have zeros in the center of the bands as well as in the middle of the gap (semiconductor)/pseudogap (graphene). Impurities with potential $V(x) = V\delta(x)$ can cause resonances at energies, where the $\mathrm{Re}\, g_0(E)$ with $1/V$ lines intersect. $|V_>| \gg D$ ($|V_<| \ll D$) illustrate strongly (weakly) attractive impurity potentials and the corresponding energies of possible impurity resonances.

$$\mathrm{Re}\, g_0(E) = 1/V \;\text{ with } |\mathrm{Im}\, g_0(E)| \ll |\mathrm{Re}\, g_0(E)|. \tag{9}$$

The solutions to these conditions can be determined graphically (cf. [24]) as has been done in Fig. 1:

Weak impurities $|V_<| \ll D$ cause resonances close to the band edges and close to the gap edge of the model semiconductor, but no resonance in the middle of graphene's pseudogap is created. To obtain an impurity resonance in the vicinity of the Fermi level of graphene, the impurity potential has to exceed a threshold $|V| \gtrsim D$ on the order of the bandwidth. Concerning weak impurities $|V_<| \ll D$, graphene behaves like the model of the metal with no resonances close to the Fermi level and turns out to be robust against perturbations of this kind. As regards strong impurities $|V_>| \gg D$ graphene exhibiting an impurity state in the center of the (pseudo)gap is more similar to the model semiconductor than to the metal. This overall behavior of graphene is directly related to its local, unperturbed Green function g_0^{g}: the divergences of $\mathrm{Re}\, g_0^{\mathrm{g}}(E)$ are the same as for metal ($g_0^{\mathrm{m}}(E)$), but the structure of zeros $\mathrm{Re}\, g_0^{\mathrm{g}}(E) \to 0$ with $\mathrm{Im}\, g_0^{\mathrm{g}}(E) \ll \mathrm{Re}\, g_0^{\mathrm{g}}(E)$ is the same as for the semiconductor ($g_0^{\mathrm{s}}(E)$).

In the latter case of a strong impurity, the energy E_{imp} of the impurity resonance and its width Γ show a universal behavior. For $|V| \gg D$, Eq. (9) simplifies to $2E_{\mathrm{imp}} \ln|\frac{E_{\mathrm{imp}}}{D}| = \frac{D^2}{V}$ and consequently [24,19,21]

$$E_{\mathrm{imp}} \approx \frac{D^2}{2V \ln|\frac{D}{2V}|}. \tag{10}$$

This resonance is well-defined if its width Γ is small as compared to the distance to the closest Van-Hove singularity: $\Gamma \ll |E_{\mathrm{imp}}|$. An expansion of Eq. (8) about E_{imp} yields $T(E) \sim \frac{1}{(E-E_{\mathrm{imp}})+i\Gamma}$ with

$$\begin{aligned}\Gamma &= \mathrm{Im} g_0^{\mathrm{g}}(E_{\mathrm{imp}}) \cdot \left(\frac{\partial \mathrm{Re}\, g_0^{\mathrm{g}}(E)}{\partial E}\bigg|_{E_{\mathrm{imp}}}\right)^{-1} \\ &\approx \frac{\pi}{2}|E_{\mathrm{imp}}|\left|\ln\left|\frac{E_{\mathrm{imp}}}{D}\right| + 1\right|^{-1}.\end{aligned} \tag{11}$$

The criterion $\Gamma \ll |E_{\mathrm{imp}}|$ is best fulfilled for $|E_{\mathrm{imp}}|$ close to the Dirac point: with increasing potential strength $V \to \infty$, the impurity resonances approaches the Dirac point $|E_{\mathrm{imp}}| \to 0$ and becomes arbitrarily sharp $\Gamma \to 0$ with $\Gamma/|E_{\mathrm{imp}}| \to 0$.

2.2. The nature of midgap impurity state

The ingredients to the discussion of the previous section were the density of states of the host material and the requirement for the impurity potential that the matrix elements are the same between all eigenstates $|k\rangle$ and $|k\prime\rangle$ of the unperturbed system. This leads to the possibly counterintuitively appearing conclusion that strong impurities $V \to \infty$ cause midgap states in graphene and in semiconductors. Indeed, the same arguments can be made for impurities in the pseudogap phase of high-Tc superconductors [25,24]. But what is the nature of these impurity states and why do they occur?

In the language of Green functions, this question has been answered already: a host with unperturbed Green function $g_0(E)$ fulfilling $\mathrm{Re} g_0(E) \to 0$ and $\mathrm{Im} g_0(E) \ll \mathrm{Re} g_0(E)$ for $E \to E_{\mathrm{imp}} = 0$ is required.

The simplest system fulfilling this requirement is a two-level system with Hamiltonian $\widehat{H} = \Delta\sigma_3$, where σ_i $(i = 1,2,3)$ are the usual Pauli matrices and σ_0 is the corresponding identity matrix. The eigenenergies of this system are $\pm\Delta$. In this system playing the role of the host, an 'impurity potential' with the matrix elements between all eigenstates of the unperturbed system being the same reads as $\widehat{V} = V(\sigma_0 + \sigma_1)$. The perturbed system $\widehat{H} + \widehat{V}$ is easily diagonalized and has eigenenergies $E_1 = 0$ and $E_2 = 2V$ in the limit $V \gg \Delta$. The state at zero energy $|-\rangle = (1,-1)/\sqrt{2}$ is the pendant of the midgap state in graphene and in the model semiconductor. So, a strong impurity forces the system into eigenstates of the impurity potential and the midgap states are those effectively decoupled $\widehat{V}|-\rangle = 0$ from the impurity operator.

This result and its atomistic meaning can be translated to case of graphene by means of the following tight-binding model. The low energy band structure of graphene is determined by electrons in the out-of-plane p-orbitals, the p_z orbitals, of the carbon atoms. In the approximation of nearest-neighbor hopping, the π-band the tight-binding Hamiltonian is [26,27]

$$\widehat{H} = t\sum_{\langle ij\rangle} a_i^\dagger b_j + a_j^\dagger b_i, \tag{12}$$

where a_i and b_i denote the Fermi operators of electrons localized in the carbon p_z orbital of sublattice atoms A and B in the cell at R_i, respectively. The sum includes all pairs of nearest-neighbor carbon atoms and $t \approx 2.7$ eV is the nearest-neighbor hopping parameter.

Using the Fourier transformed operators a_k (b_k), defined by $a_i = \int_{\Omega_B} \frac{d^2k}{\Omega_B} e^{ikR_i} a_k$ and b_i analogously, the Hamiltonian reads as $\widehat{H} = \int_{\Omega_B} \frac{d^2k}{\Omega_B} \Psi_k^\dagger H_k \Psi_k$ with $\Psi(k) = \begin{bmatrix} a_k \\ b_k \end{bmatrix}$ and the k-dependent 2×2 matrix

$$H_k = \begin{pmatrix} 0 & \xi(k) \\ \xi^*(k) & 0 \end{pmatrix}, \tag{13}$$

where $\xi(k) = t\sum_{j=1}^{3} e^{ik(b_j - b_1)}$ and b_j $(j = 1,2,3)$ are the vectors connecting neighboring atoms [28]. The 2-dimensional Hilbert space operated on by the matrices H_k describes the two sublattices in graphene. It is often called pseudospin space for its formal similarity to a spin-1/2 space coming along with the algebra of Pauli matrices σ_i, $i = 0,1,2,3$, acting on this sublattice degree of freedom. As $H_k = -\sigma_3 H_k \sigma_3$ is chiral, its spectrum is symmetric about $E = 0$ and given by $\epsilon(k) = \pm|\xi(k)|$. The positive and negative branches of this dispersion touch at the corners $K^\pm$ of graphene's Brillouin zone and exhibit linear dispersion in the vicinity. For pristine graphene, the Fermi level lies exactly at the touching point of these bands – called Dirac point.

Applying $k\cdot p$ perturbation theory to H_k near $K^\pm$ yields a long wavelength theory of electrons in graphene [28]:

$$H_{K^\pm} = v_{\mathrm{f}}\hbar(p_1\sigma_1 \mp p_2\sigma_2), \tag{14}$$

where $v_{\mathrm{f}} \approx 5.8\,\mathrm{eV\AA}/\hbar$ is the Fermi velocity. $H_{K^\pm}$ is formally the Dirac equation of massless particles with the speed of light being replaced by v_{f}. This is why the low energy electronic excitations in graphene behave like two species (at K^+ and K^-, respectively) of massless Dirac fermions as highlighted in the introduction. We will see that the chirality of the Dirac Hamiltonian manifests itself in impurity induced midgap states.

Impurities acting as potential scatterers read in this model as $\widehat{V}_{\mathrm{pot}} = \sum_{i,j} \Psi_i^\dagger V_{i,j} \Psi_j$, with $V_{i,j}$ being complex 2×2 matrices. The eigenstates of H_k (and $H_{K^\pm}$) are of the form $|k_\pm\rangle \sim (1, e^{i\phi(k)})$ with $\phi(k) \in [0, 2\pi)$. Therefore, impurities as discussed in Section 2.1 with the matrix elements being the same between all eigenstates of the unperturbed Hamiltonian translate into this model as potentials localized at the origin and acting on one sublattice only: $V_{0,0} = V_{\mathrm{s}} = U_0 \begin{pmatrix} 1 & 0 \\ 0 & 0 \end{pmatrix}$, for a 'single' impurity in sublattice A with potential strength U_0.

The Green function formalism introduced in Section 2.1 can be directly applied to this tight-binding model of graphene with Eq. (8) involving now 2×2 matrices in sublattice space rather than complex numbers. The local Green function appearing in this context is $g_0(E) = \int_{\Omega_B} \frac{d^2k}{\Omega_B} (E - H_k + i\delta)^{-1}$.

Impurity resonances occur at $\mathrm{Re}\det T(E_{\mathrm{imp}}) = 0$ (see [21]) and a comparison of resonant energies E_{imp} in this tight-binding model to

the purely DOS based model shows that single localized impurities acting one sublattice behave quasi identical in both models (see Fig. 2). E_{imp} approaches the Dirac point for $U_0 \to \infty$ in the same manner in both models. The importance of the atomistic structure of the impurity for the creation of this midgap state can be inferred from the resonant energies of impurity states due to 'double impurities' $V_{0,0} = V_{\mathrm{d}} = U_0 \begin{pmatrix} 1 & 0 \\ 0 & 1 \end{pmatrix}$ acting on both sublattices within the unit cell at the origin.

This pair of neighboring scatterers produces a resonance at the Dirac point for $U_0 = 3t \approx 8.1$ eV and E_{imp} changes sign, when U_0 passes through this value. This is in contrast to a single impurity, where $E_{\mathrm{imp}} \to 0$ appears only in the limit of infinite potential strength and changing the sign of E_{imp} requires changing the sign of U_0.

This universal behavior of the single impurity is closely related to the real space shape of the created midgap state, i.e. the site dependence of impurity induced changes in the LDOS. In the tight-binding formalism from above, the LDOS (as is the Green function) at a site i is 2×2 matrix $N(i,E) = -\frac{1}{\pi}\mathrm{Im}G(i,i,E)$ in sublattice space. Its diagonal elements contain the LDOS projected on sublattice A (B) of the unit cell located at R_i. Introducing wave functions $\Phi_i(r)$ for the carbon p_z orbitals, this discrete LDOS can be converted to the continuous r-dependent LDOS $N(r,E) = -\frac{1}{\pi}\mathrm{Im}\left(\sum_{i,j}\Phi_i(r)G(i,j,E)\Phi_j^{\dagger}(r)\right)$.

The LDOS in the vicinity of single and double impurities with resonances at $E_{\mathrm{imp}} = -0.1$ eV are shown in Fig. 3. A strong single impurity in sublattice A induces an impurity state mostly localized in sublattice B and vice versa. A state localized in one sublattice can only be realized close to the Dirac point $E = 0$, as chirality of the Hamiltonian requires

$$E_{\mathrm{imp}}\begin{pmatrix}1\\0\end{pmatrix} = H_k\begin{pmatrix}1\\0\end{pmatrix} = -\sigma_3 H_k \sigma_3\begin{pmatrix}1\\0\end{pmatrix} = -E_{\mathrm{imp}}\begin{pmatrix}1\\0\end{pmatrix}. \tag{15}$$

This result can be also viewed as manifestation of Lieb's theorem [29] in graphene: having an infinitely strong potential acting at one site means decoupling this site from the rest of the system and thus having different numbers of atoms in sublattices A and B: $N_{\mathrm{A}} \neq N_{\mathrm{B}}$. Lieb's theorem states that any repulsive Hubbard model on a bipartite lattice will have a ground state with spin $S = 1/2|N_{\mathrm{A}} - N_{\mathrm{B}}|$. So, the impurity state with $E_{\mathrm{imp}} \to 0$ is the host of this magnetic moment.

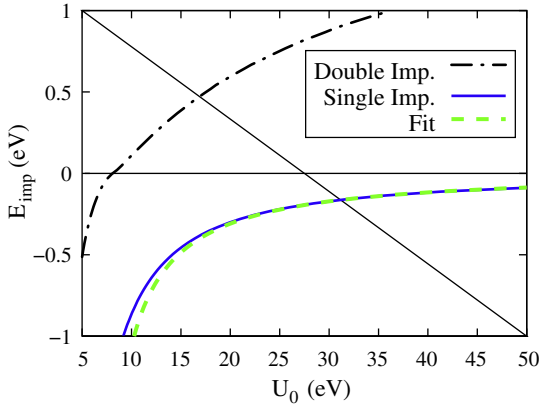

Fig. 2. Relation between the atomic strcuture of the impurity and the energy E_{imp} of the impurity resonances: for single and double impurities, E_{imp} is shown as function of the potential strength U_0. For the single scatterer E_{imp} obtained from the tight-binding model is compared to the result obtained from the DOS based model from Section 2.1. (Eq. (10) with fitted bandwidth $D = 6.06$ eV and $V = U_0$.) In the limit of strong potentials $U_0 \to \infty$, single impurities cause a universal midgap state, $E_{\mathrm{imp}} \to 0$. This is a consequence of chiral nature of the graphene Hamiltonian (see text) and in contrast to the case of double impurities. From [21].

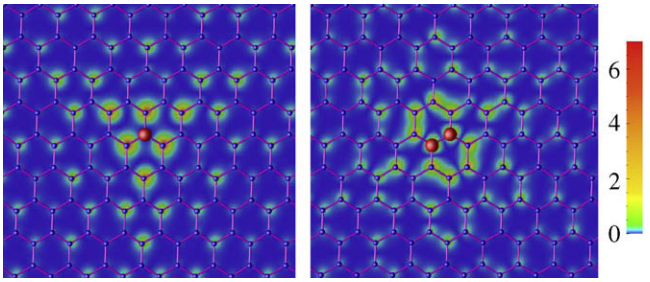

Fig. 3. Real space properties of impurity states for different atomic structures of the impurity: the r-dependent LDOS at $E = E_{\mathrm{imp}} = -0.1$ eV is shown for a single impurity with $U_0 = 45$ eV (left) and for a scalar double impurity with $U_0 = 6.9$ eV (right) encoded corresponding to the color bar. The impurity sites are marked as big red dots in the center of the images. The impurity state due to the single impurity in one sublattice is almost entirely localized in the other sublattice. Such a state can only exist very close to the Dirac point (see Eq. (15)). From [21].

Scanning tunneling microscopy (STM) allows to image impurity states with very high spatial resolution. This so-called 'wave function imaging' yields local images of the impurity induced wave function and has been realized, e.g., for graphite surfaces [30–33]. The symmetry of graphene's electronic states at the Fermi level results in the impurity states depending strongly on microscopic details of the impurity like the adsorption site. As Fig. 3 shows, single and double impurities can be distinguished by the symmetry of the induced impurity state even if the resolution of the STM is not sufficient to resolve the difference between single and double impurities, directly.

Investigating the effect of impurities in graphene on the length scale of the lattice constant requires H_k from Eq. (13) as description of the pristine system, whereas at larger length scales $H_{K^{\pm}}$ from Eq. (14) suffices as unperturbed starting point. Using this linearized Hamiltonian, the diagonal part of graphene's unperturbed real space Green function simplifies to

$$g_0(r,\omega) = \omega v_{\mathrm{f}}^2 \int \mathrm{d}p \frac{pJ_0(pr)}{D^2(\omega^2 - v_{\mathrm{f}}^2 p^2)}$$

for large distances $r \gg \hbar v_{\mathrm{f}}/\omega$ from the impurity site [34]. (D parametrizes the graphene bandwidth.) As a consequence, the changes in LDOS decay according to a power law $\Delta N(r, E_{\mathrm{imp}}) \propto 1/r$ for $E_{\mathrm{imp}} \neq 0$ as found by several authors [17,35,21]. A hard-wall impurity, i.e. $U_0 \to \infty$ and $E_{\mathrm{imp}} = 0$, has $1/r^2$ asymptotics of $\Delta N(r, E_{\mathrm{imp}})$ [36].

2.3. Resonant impurities

So far, we considered impurities acting as potential scatterers in graphene. Many impurities contribute orbitals, $\widehat{H}_{\mathrm{imp}} = \epsilon_{\mathrm{imp}} d^{\dagger} d$, with Fermi operator d and energy ϵ_{imp} which hybridize with the graphene bands, $\widehat{V} = \sum_i \Psi_i^{\dagger} V_i d + \mathrm{h.c.}$ This problem has been extensively discussed for normal metals and is often referred to as 'non-interacting Anderson impurity model' [37].

Changing to the momentum space representation $\widehat{V} = \int_{\Omega_B} \frac{d^2k}{\Omega_B} \Psi_k^{\dagger} V_k d + \mathrm{h.c.}$ and evaluating the appropriate matrix elements in Eq. (2) leads to

$$(E - \epsilon_k) G_{k,k'}(E) = \delta_{k,k'} + \sum_{k''} \frac{V_{k'}^* V_{k''}}{E - \epsilon_d} G_{k'',k'}(E) \tag{16}$$

and

$$(E - \epsilon_d) G_{d,d}(E) = 1 + \sum_k \frac{|V_k|^2}{E - \epsilon_k} G_{d,d}(E), \tag{17}$$

where $k = (k, \pm)$ includes crystal momentum k and band index $\pm$. Eq. (16) shows that a resonant impurity acts on the graphene electrons like an energy dependent potential

$$V_{k,k'}(E) = \frac{V_{k'}^* V_{k''}}{E - \epsilon_d}. \quad (18)$$

Hence, all results for the potential impurities can be translated to resonant impurities. Combining Eqs. (10) and (18) yields possible resonant energies E_{imp} with corresponding resonance width Γ according to Eq. (11). Well-defined impurity resonances with significant spectral weight in the graphene bands require that $\Gamma \ll |E_{\mathrm{imp}} - \epsilon_d|$, i.e. that the singularity in the effective potential, Eq. (18), is well separated from the resonance.

An adsorbate having an orbital close to the Dirac point ($|\epsilon_d| \ll D$), which is strongly bond to one carbon atom in one sublattice only ($V_k = V \gtrsim D$), fulfills this condition and will act like a very strong static impurity potential in the vicinity of the Dirac point. A chiral midgap state with $|E_{\mathrm{imp}}| < |\epsilon_d|$ is created. A weakly hybridized impurity orbital ($V_k = V \to 0$) will lead to $E_{\mathrm{imp}} \to \epsilon_d$ and $|E_{\mathrm{imp}} - \epsilon_d| < \Gamma$. No strong resonance in the graphene bands will occur. However, depending on its filling a weakly hybridized impurity orbital can act as donor or acceptor level and create a charged impurity.

2.4. Clusters and extended impurities

The impurities considered so far acted on the length scale of the graphene lattice constant and graphene prove insensitive to single weak perturbations at this length scale. We briefly turn now to potentials acting over on bigger areas of the graphene sheet, which are smooth on the atomic scale. Such potentials are diagonal in the sublattice indices and enter the tight-binding model as $\widehat{V}_{\mathrm{pot}} = \sum_i V_i \Psi_i^\dagger \Psi_i$, with V_i being a real number varying slowly with site index i. Transferring to the long wavelength Dirac formalism yields smooth scalar potentials $V(r)\sigma_0$. Such potentials shift the Dirac point locally, i.e. they lead to local doping if either the surrounding graphene sheet or the substrate can act as reservoir for electrons or holes. In this sense, weak extended potentials may strongly influence the electronic properties of a graphene sample.

Besides these local doping effects, graphene's electronic properties turn out to be insensitive also to these extended potentials: as these potentials are diagonal in sublattice space, they cannot change the sublattice isospin of charge carriers upon scattering. This leads to a strong suppression of backscattering of electrons off potential barriers and all smooth barriers becoming fully transparent for electrons at normal incidence [38].

3. Realistic impurity effects

To understand which of the interaction mechanisms discussed in the previous section is effective for which impurity present in real graphene samples, one needs to remember fundamental differences between open-shell (like alkali ad-atoms) and closed-shell impurities (like H_2O adsorbates or noble gas ad-atoms): closed-shell molecules or atoms are chemically rather inert and exhibit gaps between their highest occupied molecular orbitals (HOMO) and their lowest unoccupied molecular orbitals (LUMO) typically on the order of $E_{\mathrm{HL}} \approx 5 - 10$ eV. For these adsorbates to contribute additional molecular orbitals in the vicinity of graphene's Dirac point, a chemical potential mismatch between molecule and graphene of the same order of magnitude is required. For open-shell systems the situation is reversed: as one orbital is only partially populated, occupied and unoccupied states are separated by Hund exchange of the order of $E_{\mathrm{HL}} \approx 1$ eV. Thus, any open-shell adsorbate can be expected to come along with additional molecular orbitals close to the Dirac point of graphene, which may hybridize with the graphene bands, become charged and directly cause doping, etc. In the following we will discuss effects by open- and closed-shell adsorbates separately.

3.1. Open-shell impurities

As examples of open-shell impurities, NO_2 and K adsorbed on graphene have been investigated by means of angular resolved photo emission (ARPES) as well as in transport experiments. ARPES with graphene on SiC observed lifting (lowering) of the chemical potential upon K (NO_2) exposure [39,40] and showed that these adsorbates act as donor and acceptor, respectively. Similarly transport experiments with back gated graphene on SiO_2 substrates, measured the electric field effect in graphene and found doping due to NO_2 and K adsorbates [22,41]. This doping turned out to reversible: annealing the samples at 420 K for NO_2 and at 490 K for potassium removed the doping and recovered the samples to their pristine state. NO_2 and K appear to be weakly bound but cause strong doping. This is quite in contrast to adsorbates like atomic hydrogen which require considerably higher temperatures (720 K) to be removed from graphene [42]. We firstly discuss easily removable and charge donating/accepting impurities like K and NO_2 and continue with rigidly bond impurities like H.

Density functional theory simulations on NO_2 interacting with graphene showed that NO_2 physisorbs on graphene and gives rise to acceptor levels [23]: NO_2 maintains equilibrium with its dimer N_2O_4, with both adsorbing to graphene in various different geometries. Fig. 4 shows fully relaxed adsorbate configurations and the associated electronic DOS.

The spin-polarized DOS of graphene with adsorbed NO_2 reveals an acceptor level at 0.4 eV below the Dirac point, independent of adsorption geometry. The molecular orbitals of NO_2 manifest themselves as peaks in the DOS. The acceptor level is formed from the partially occupied molecular orbital (POMO) of NO_2, which is split by a Hund-like exchange interaction: its spin-majority component lies approximately 1.5 eV below the Dirac point and is fully occupied

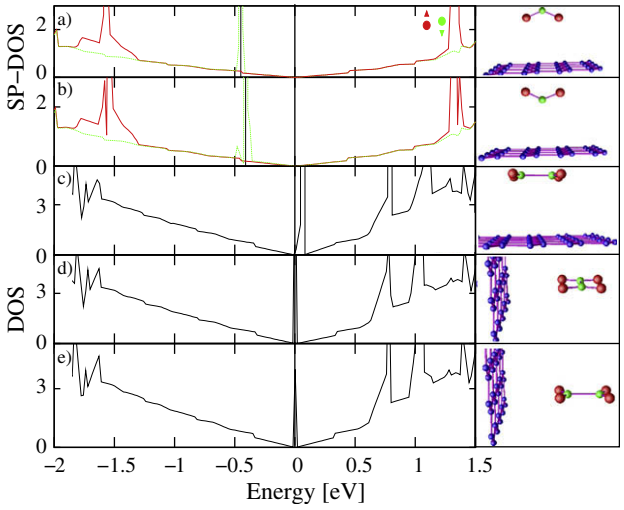

Fig. 4. Interaction of NO_2 and N_2O_4 adsorbates with graphene and associated doping mechanisms. Left: spin-polarized DOS of the graphene supercells with NO_2, (a–b), and DOS of graphene with N_2O_4, (c–e). The partially occupied NO_2 molecular orbital results in a peak in the DOS at approx. −0.4 eV and acts as an acceptor level. Similarly the N_2O_4 LUMO manifests as a peak in the DOS slightly above $E = 0$ and can accept thermally excited electrons. The energy of the Dirac points is defined as $E_D = 0$. In the case of NO_2 the Fermi level E_f of the supercell is below the Dirac point, directly at the energy of the spin down POMO. For N_2O_4, $E_f = 0$ is at the Dirac point. Right: adsorption geometries obtained in density functional theory. The carbon atoms are printed in blue, nitrogen green and oxygen red. The DOS are mainly independent of adsorption geometry, which is characteristic for weakly hybridized impurities. From [23].

on graphene as well as for the free NO_2 molecule. The minority spin component of the NO_2 POMO is unoccupied for free NO_2, but 0.4 eV below the Dirac point in the adsorbed configuration – it gets populated by electrons from graphene. Band structure calculations allow to extract the hybridization of the NO_2 acceptor bands with the graphene bands and yield $V_k/D < 0.1$ for V_k as entering Eq. (18). The acceptor level is weakly hybridized with the graphene bands and localized at the NO_2 adsorbate.

For N_2O_4 the situation is similar: its lowest unoccupied molecular orbital (LUMO) is always quite near to the Dirac point, i.e. between 1 meV and 66 meV above it, and also weakly hybridized with the graphene bands. This initially empty N_2O_4 LUMO can be populated by the graphene electrons due to thermal excitations and can consequently act as an acceptor level. So, density functional theory predicts acceptor levels far below and rather close to the Dirac point caused by the NO_2 monomer and the dimer, respectively.

Hall effect measurements suggest [23] that there are indeed two types of dopants, when graphene is exposed to NO_2: Outside the charge neutrality region the inverse Hall resistance $1/R_{xy} \sim (n-p)$ is proportional to the concentration of holes (p)/ electrons (n) in the graphene sample. Fig. 5 shows $1/R_{xy}$ measured at $B = 1\,T$ as a function of the gate voltage V_G with and without NO_2 on top of back gated graphene devices on SiO_2. Two characteristic shifts – one for all V_G and an additional shift above the charge neutrality region – occur upon NO_2 exposure. A deep acceptor level causes a solid shift at all V_G, while an acceptor level close to the Dirac point gives rise to an additional shift of the electron branch (straight line at negative $1/R_{xy}$). Therefore, these Hall effect measurements strongly support the DFT result of two distinct impurity levels due to NO_2 and N_2O_4.

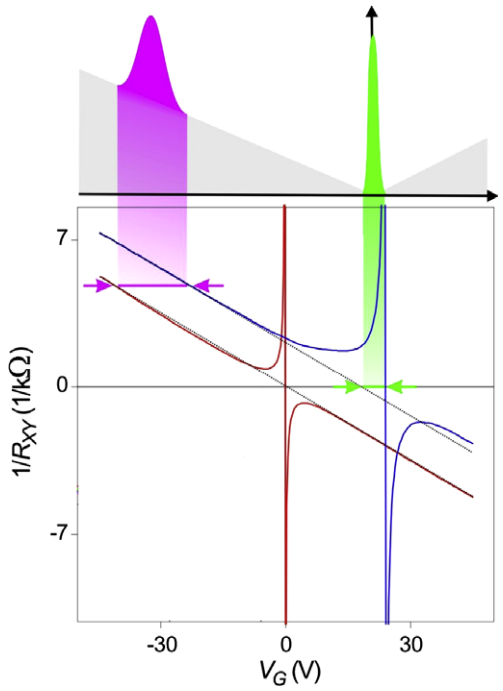

Fig. 5. Manifestation of NO_2 and N_2O_4 induced acceptor levels in Hall effect measurements. The inverse Hall resistance, $1/R_{xy} \sim (n-p)$ is a measure for the concentration of mobile holes, p, and electrons, n, in the sample. $1/R_{xy}$ as function of gate voltage, V_G, is shown for pristine (red curve) and doped (blue curve) graphene samples in the lower panel. The blue curves exhibits two characteristic shifts w.r.t. the red curve indicated by green and magenta arrows. These shifts can be related to the DOS of doped graphene shown in the upper panel. Here, grey depicts the DOS for pure graphene, the magenta peak represents the DOS for NO2 and green peak the N_2O_4 acceptor level. The deep NO_2 acceptor level causes a rigid shift of the $1/R_{xy}$ vs. V_G curves at all gate voltages, whereas the N_2O_4 induced acceptor level results in an additional shift close to zero gate voltage. From [23].

In the limit of exposure to NO_2 strongly diluted in an inert gas atomsphere, Schedin et al. [22] detected characteristic jumps in the Hall resistivity of their graphene devices corresponding to single electrons being removed or introduced to the sample. As NO_2 appears to create one deep acceptor level, these jumps correspond to the detection of single NO_2 molecules and support the picture that one electron is transferred from graphene to NO_2 per adsorbate molecule.

NO_2 molecules cause doping but do not create any chiral midgap state in graphene. So, they are one example of the class of charged, weakly hybridized impurities, as discussed in Section 2.3. DFT calculations find that alkali and halogen ad-atoms (except for fluorine) belong to the same class, being donors and acceptors, respectively [43,44]. These impurities exhibit adsorption energies within the wide range of $0.05 - 1$ eV but their migration barriers do not exceed 0.1 eV (except for Li). Ionically bond impurities can be therefore expected to be strongly mobile on graphene at room temperature. This impurity mobility explains why K or NO_2 doped graphene can be easily annealed to its pristine state and is being debated as one possible explanation of seemingly contradictory experiments:

Room temperature experiments with NO_2 of Schedin et al. [22] find hole doping up to concentrations of 1.5×10^{12} cm^{-2} and the electron mobility staying constant within 20% of its mean value. The charged NO_2 impurities do not seem to strongly affect electron scattering. However, depositing K on graphene at cryogenic temperatures [41], Chen et al. achieved electron doping up to $5 - 6 \times 10^{12}$ cm^{-2} but found the electron mobility decreasing by more than a factor of 15 within this doping range. Even for dopant concentrations inside the range of the experiment by Schedin et al., Chen et al. find decreasing electron mobility. Clustering of impurities strongly suppresses their contribution to the resistivity of graphene [45]. Therefore, NO_2 being mobile at room temperature might have formed clusters, whereas K is immobile at cryogenic temperatures and clustering might not have taken place at these conditions.

The charged impurities discussed so far are strong dopants and limit the electron mobility under certain conditions. There is, however, another class of open-shell impurities contributing significantly to electron scattering in currently studied graphene samples: transmission electron microscopy (TEM) allows one to visualize atomic scale defects in graphene samples of a few 10 nm in size. Using this technique, Meyer et al. [46] found hydrogen ad-atoms sticking rigidly on graphene and being immobile at room temperature. This is in strong contrast to the ionically bond impurities discussed before.

The nature of bonding of H-atoms to graphene has been studied by means of density functional theory calculations [47,48]. In its minimum energy configuration the H atom sits on top of a carbon atom. The LDOS at this carbon atom (Fig. 6) is strongly redistributed: it decreases in the region between −2.5 and +5 eV around the Fermi level and increases near ±7 eV. These changes correspond to a transition from sp^2 to sp^3 hybridization. The carbon atom next to H forms a σ bond with the H ad-atom and the π bonds to its nearest carbon neighbors are broken. Thus, the bonding partner of H is decoupled from the graphene π-electron system and there is a local imbalance between the number of atoms belong to each of the two sublattices.

In this sense, a hydrogen ad-atom realizes the situation of a strong impurity acting on one sublattice only, which has been discussed in terms of a tight-binding model in Section 2.2. The LDOS at nearest-neighbors of the carbon atom bonding to hydrogen (Fig. 6) shows a midgap peak, which is a manifestation of the $V \to \infty$ universal midgap state discussed in terms of the tight-binding model. In this picture, a hydrogen ad-atom and a vacancy have the same effect on the graphene π- electrons. Band structure calculations showed that covalently bound monovalent impurities

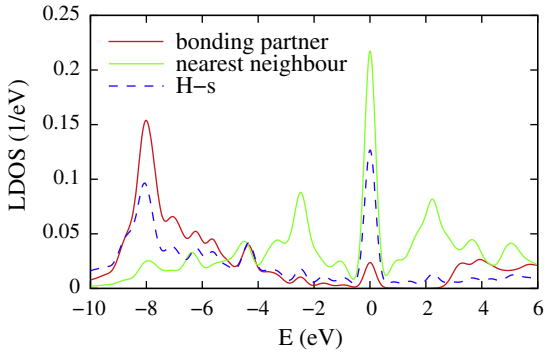

Fig. 6. The local electronic structure in the vicinity of a hydrogen adatom. The LDOS at the adatom as well as the p_z projected LDOS for the impurity's bonding partner in graphene and its nearest-neighbor the are shown. A midgap state contributing significant spectral weight at the H adatom and at nearest-neighbor of its bonding partner but not at the bonding partner directly is apparent. The nature of this midgap state is same as for strong single impurity with $|U_0| \gg D$ depicted in Figs. 2 and 3. From [44].

like OH, F or CH_3 groups, in general, tend to sit on top of one carbon atom and decouple this atom from graphene's Dirac bands [44]. Therefore, all covalently bound monovalent impurities scatter electrons in the same way vacancies do. A quantitative study by Robinson et al. confirms this qualitative statement [49] by mapping out the parameters entering the non-interacting Anderson impurity model, Eq. (18), from band structure calculations. They find $V_k \approx D$ for H and OH bound to graphene.

DFT calculations show that a clear distinction between ionic and covalent bonding is possible for all monovalent impurities [44]. All monovalent covalently bound impurities cause a midgap state which contributes a few percent to the spectral weight at the adsorbate. Strongly electronegative adsorbates result in the midgap state being slightly below the Dirac point of graphene and make this state act as an acceptor level, although it is mainly derived from carbon orbitals. F and OH induced midgap states accept on the order of one electron, whereas H and CH_3 result in neutral midgap states. Migration of impurities with neutral midgap states is strongly suppressed: at half-way from one carbon atom to the next, a covalent bond of the impurity to the two neighboring carbon atoms is highly unfavorable. As a result, there is a high energy barrier (on the order of 0.5–1 eV) if the adsorbate cannot become charged and form a ionic bond in this saddle point configuration [44]. This barrier explains the high stability of H ad-atoms on graphene seen in TEM [46].

3.2. Inert impurities

Experiments show that graphene is sensitive to closed-shell molecules like H_2O, NH_3 and CO: Schedin et al. found that these adsorbates cause doping of graphene [22]. DFT calculations with H_2O adsorbed on graphene in concentrations of 1 H_2O per 32 carbon atoms [50] predicts H_2O to physisorb at 3—4 Å above the graphene sheet with adsorption energy on the order of $\lesssim 50$ meV. However, there are no changes in the DOS close to the Fermi level upon adsorption of the molecule. The HOMO and LUMO of the H_2O are both more than 2 eV away from the Fermi level (Fig. 7a). This absence of impurity levels close to the Dirac point shows that single water molecules on perfect free-standing graphene sheets do not cause any doping. The same result is obtained for the adsorption of single NH_3 molecules on graphene [50,51]. None of these adsorbates act as direct dopants.

The H_2O induced doping [2,22] is thus due to more complicated mechanisms. The experiments dealing with water induced doping used graphene on top of substrates like SiO_2, which can be crucial for achieving doping. In addition, H_2O clusters might form. In the following we show how in both cases the electric field due to the H_2O dipole can shift bands and cause doping.

The limiting case of large H_2O clusters can be modelled as ice overlayers on graphene. Ice Ih, the ordinary form of ice, has been proposed as basis of ice growth on hexagonal metal surfaces [52] and layers of this modification are almost commensurate with a

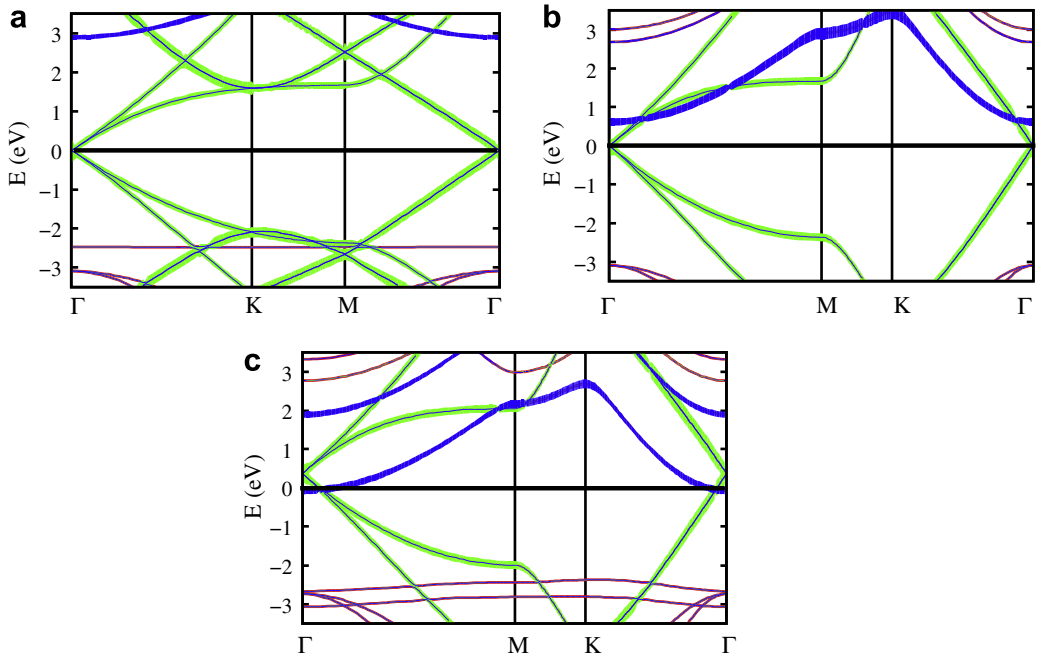

Fig. 7. Influence of H_2O adsorption on the electronic structure of free-standing graphene. The band structures of supercells with fully relaxed single H_2O molecules (a), a bilayer (b) and a tetralayer (c) of ice Ih on graphene are shown. The graphene π bands are marked in green, the nearly free electron bands in blue. Due to the H_2O dipole moments, graphene's nearly free electron band is shifted with respect to its π bands. This shift w.r.t. the pristine state increases from (a) to (c), i.e. with H_2O concentration. To achieve hole doping, a shift on the order of 3 eV is required. This large shift is only reached for four layers of proton ordered ice Ih on graphene. From [54].

$(\sqrt{3} \times \sqrt{3})R30^{\circ}$ graphene supercell: the lattice mismatch is 0.23 Å. Ice Ih is a hexagonal crystal of water molecules constructed according to the so-called 'Bernal–Fowler–Pauling' rules [53], which allow for orientational disorder of the molecules. Ice in absence of such disorder is called 'proton ordered ice' and causes the highest dipole induced electric fields among all ice Ih structures.

DFT simulations comparing single H_2O, with bi- and tetralayers of proton ordered ice Ih on graphene [54] show that the electric fields generated by the overlayers are strong enough to significantly change the energy of graphene's nearly free electron bands. The supercell bandstructures (Fig. 7) show that these electric fields shift the nearly free electron bands down from more than 3 eV above the Dirac point for pristine graphene or graphene with very few H_2O adsorbates to 0.6 eV above and 0.1 eV below the Dirac point for a bi- and a tetralayers of ice Ih, respectively.

Thus, hole doping for a tetralayer of proton ordered ice on free-standing graphene is found to be possible with graphene's nearly free electron bands acting as reservoir of holes. However, a comparison of changes in contact potential in the simulation to those measured by electrostatic force microscopy (EFM) shows that this ice induced doping mechanism is not the most dominant in today's samples [55,54].

The above mechanism required shifting of graphene's nearly free electron bands by as much as 3 eV to have a reservoir of holes, but on a substrate with electronic states closer to the Fermi level, smaller shifts suffice to achieve doping. Defects in SiO_2 substrates are, e.g., one source of states close to the Fermi level and are likely present in many experiments. The SiO_2 surfaces in the experiments are amorphous and exhibit so-called Q_3^0 defects [56] consisting of under coordinated silicon atoms. The (111) surface of β-cristobalite, a crystalline phase of SiO_2, allows for creating the same defects, is almost commensurate with a 2×2 graphene supercell and has been used in DFT simulations [54]. The Q_3^0 defects cause impurity bands within ± 1 eV around the Fermi level of the graphene-SiO_2 systems, as Fig. 8a and d show. Without adsorbates the impurity bands do not cross the Fermi level. However, H_2O in between graphene and the substrate changes this situation (Fig. 8c, e and f) and leads to doping in this way. The DFT simulations in [54] demonstrate that these defect states are susceptible enough to the H_2O dipole electric fields to act as reservoirs for electrons and holes.

This microscopic view of electrons being pushed to the substrate is well in line with EFM [55]: the graphene contact potential changes by about +1 V upon water adsorption (exposure to moist N_2 with 50% relative humidity), whereas the SiO_2 substrate contact

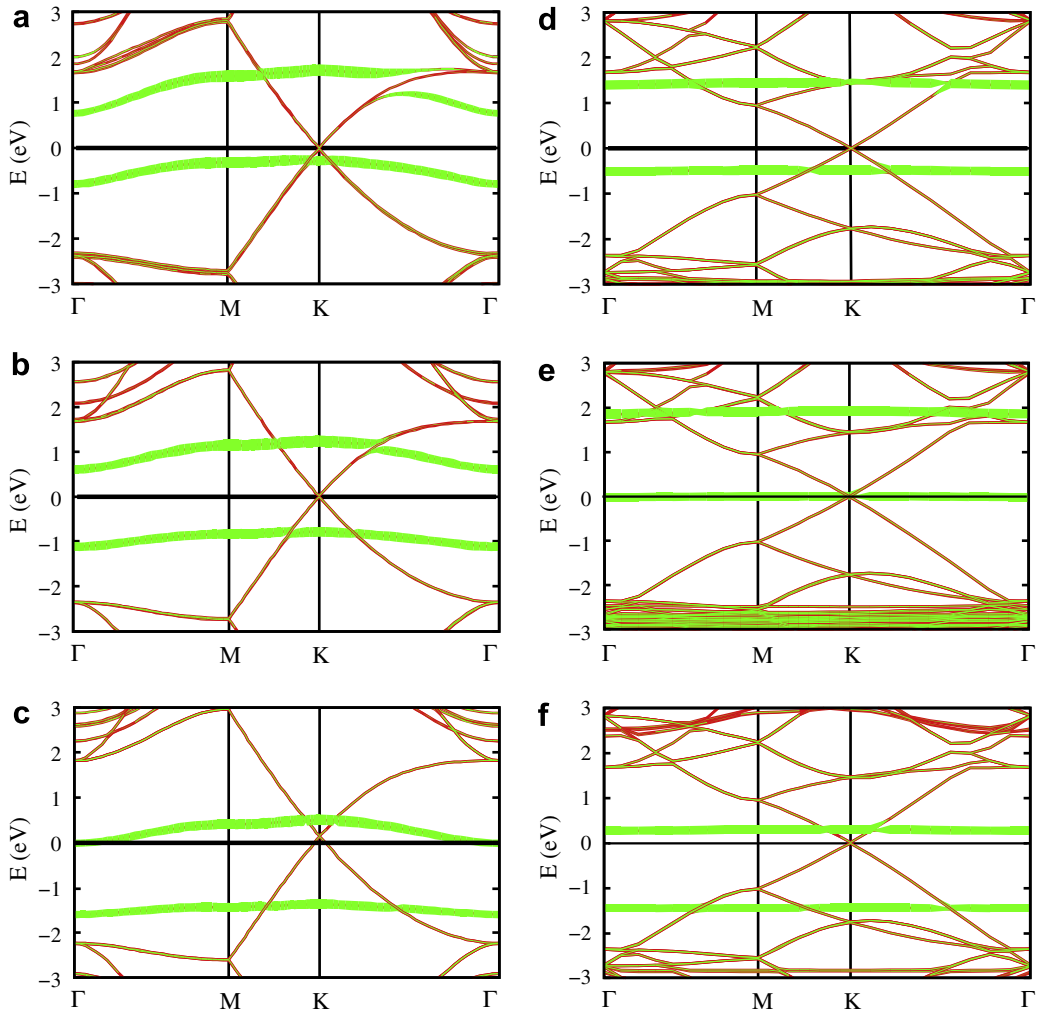

Fig. 8. Substrate mediated doping of graphene by H_2O adsorbates. The band structures for graphene on defective SiO_2 substrates with different defect and H_2O adsorbate concentrations are shown: (a–c) 2×2 and (d–f) 4×4 graphene supercells with every second, (a–c), or eighth, (d–f) surface Si atom forming a Q_3^0 defect. Spin up and down bands are shown at the same time. Contributions at the defect site are marked as green fatbands. (a) and (d) without water adsorbates. (b) with water on top of graphene. (c), (e), and (f) with water between graphene and the substrate. To illustrate the importance of the adsorption geometry different adsorbate orientations are considered: (c), (f) H_2O dipole moment pointing tilted towards the substrate. (e) H_2O dipole moment pointing towards graphene. The H_2O dipole field shifts the impurity bands of the substrate relative to the graphene bands, which can lead to hole doping as in (c) or electron doping (e). From [54].

potential stays almost constant during this procedure. This change in contact potential $\Delta\phi$ can be converted into doping of graphene (expressed in terms of a surface charge density σ) knowing the separation d of the compensation charges in the substrate from the graphene sheet: $\sigma = \epsilon_0\epsilon_r\Delta\phi/d \approx 2 \times 10^{13}\text{e}\cdot\text{cm}^{-2}$ for $d = 1$ nm and $\epsilon_r = 3.9$, which is the dielectric constant of SiO_2. Typical experimental values $\sigma \sim 10^{12}\text{e}\cdot\text{cm}^{-2}$ suggest $d \sim 20$ nm.

The DFT simulations as well as the EFM experiments suggest that H_2O induced doping is mediated by electrostatic dipole fields and that the separation between the compensation charges and the graphene sheet is significantly larger than the typical 2 Å found, e.g., for doping by K ad-atoms. This difference can be expected to manifest in electron scattering with indirect dopants leading to much weaker scattering than direct dopants. In the language of simple models, the inert impurities turn out act like smooth potentials and locally change the energy of the Dirac point, as discussed in Section 2.4.

4. Conclusions

We explained how impurities can interact with graphene and saw that the Dirac nature of the graphene electrons makes this material surprisingly inert against external perturbations. Weak potentials or weakly hybridized impurities do not cause any localized impurity states in graphene. This class of weak impurities includes inert closed-shell adsorbates like H_2O, which influence graphene by redistributing electrons within graphene or between graphene and its substrate. Substrate-dependent doping [57] and possibly electron-hole puddles, i.e. spatially varying chemical potentials as observed in [58,59], are consequences of these impurities. Open-shell adsorbates are very reactive. NO_2, alkali and halogen ad-atoms (except for flourine), e.g., act as direct dopants. They accept or donate one electron, bind ionically to graphene but hybridize weakly with the graphene bands and experience very low migration barriers. This is in contrast to the class of strongly hybridized covalently bond adsorbates, including H and OH, which are very stable on graphene and which can induce universal midgap states. High migration barriers for these impurities [44] make the midgap state appear as a natural candidate [12,13] for limiting the electron mobility in present graphene samples [6,7].

Impurity effects in graphene are becoming used in various different ways. Several groups demonstrated graphene-based gas sensors with high sensitivity [22] and promising operational properties [60]. Moreover, adsorbates on graphene can be used to create new two dimensional materials out of graphene and tailor its electronic properties. Large amounts of H adsorbates have been shown to change graphene to graphane and open a transport gap [42]. Finally, graphene is becoming available for local probe experiments like scanning tunneling spectroscopy or high resolution photoemission spectroscopy. In this context, graphene will present a unique substrate for studying strongly correlated impurities including magnetic ad-atoms such as Mn, Fe, or Co. Graphene's special density of states and its highly symmetric Fermi points make this material very different from widely studied metal surfaces like Cu, Ag or Au.

Acknowledgements

The authors thank A. Geim, K. Novoselov, and A. Balatsky for useful discussions. This work was supported by FOM (The Netherlands) and SFB 668 (Germany).

References

[1] R.E. Smalley, Discovering the fullerenes, in: I. Grenthe (Ed.), Nobel Lectures in Chemistry 1996–2000, World Scientific Publishing Co., 2003.
[2] K.S. Novoselov et al., Science 306 (2004) 666.
[3] A.K. Geim, K.S. Novoselov, Nat. Mat. 6 (2007) 183.
[4] M.I. Katsnelson, Mat. Today 10 (2007) 20.
[5] A.H. Castro Neto, F. Guinea, N.M.R. Peres, K.S. Novoselov, A.K. Geim, Rev. Mod. Phys. 81 (2009) 109.
[6] K.I. Bolotin et al., Solid State Commun. 146 (2008) 351.
[7] X. Du, I. Skachko, A. Barker, E.Y. Andrei, Nat. Nano. 3 (2008) 491.
[8] K.S. Kim et al., Nature 457 (2009) 706.
[9] K. Nomura, A.H. Mac Donald, Phys. Rev. Lett. 96 (2006) 256602.
[10] T. Ando, J. Phys. Soc. Japan 75 (2006) 074716.
[11] S. Adam, E.H. Hwang, V. Galitski, S. Das Sarma, Proc. Natl. Acad. Sci. USA 104 (2007) 18392.
[12] M.I. Katsnelson, K.S. Novoselov, Solid State Commun. 143 (2007) 3.
[13] T. Stauber, N.M.R. Peres, F. Guinea, Phys. Rev. B 76 (2007) 205423.
[14] M.I. Katsnelson, A.K. Geim, Phil. Trans. Roy. Soc. A 366 (2008) 195.
[15] K.S. Novoselov et al., Nature 438 (2005) 197.
[16] Y. Zhang, Y.-W. Tan, H.L. Stormer, P. Kim, Nature 438 (2005) 201.
[17] C. Bena, S.A. Kivelson, Phys. Rev. B 72 (2005) 125432.
[18] N.M.R. Peres, F. Guinea, A.H.C. Neto, Phys. Rev. B 73 (2006) 125411.
[19] Y.V. Skrypnyk, V.M. Loktev, Phys. Rev. B 73 (2006) 241402 (R).
[20] V.V. Cheianov, V.I. Fal'ko, Phys. Rev. Lett. 97 (2006) 226801.
[21] T.O. Wehling, A.V. Balatsky, M.I. Katsnelson, A.I. Lichtenstein, K. Scharnberg, R. Wiesendanger, Phys. Rev. B 75 (2007) 125425.
[22] F. Schedin, A.K. Geim, S.V. Morozov, E.W. Hill, P. Blake, M.I. Katsnelson, K.S. Novoselov, Nat. Mat. 6 (2007) 652.
[23] T.O. Wehling, K.S. Novoselov, S.V. Morozov, E.E. Vdovin, M.I. Katsnelson, A.K. Geim, A.I. Lichtenstein, Nano Lett. 8 (2008) 173.
[24] A.V. Balatsky, I. Vekhter, J.-X. Zhu, Rev. Mod. Phys. 78 (2006) 373.
[25] R. Joynt, J. Low Temp. Phys. 109 (1997) 811.
[26] P.R. Wallace, Phys. Rev. 71 (1947) 622.
[27] S. Reich, J. Maultzsch, C. Thomsen, P. Ordejón, Phys. Rev. B 66 (2002) 035412.
[28] G.W. Semenoff, Phys. Rev. Lett. 53 (1984) 2449.
[29] E.H. Lieb, Phys. Rev. Lett. 62 (1989) 1201.
[30] H.A. Mizes, J.S. Foster, Science 244 (1989) 559.
[31] K.F. Kelly, D. Sarkar, G.D. Hale, S.J. Oldenburg, N.J. Halas, Science 273 (1996) 1371.
[32] K.F. Kelly, E.T. Mickelson, R.H. Hauge, J.L. Margrave, N.J. Halas, PNAS 97 (2000) 10318.
[33] T. Matsui, H. Kambara, Y. Niimi, K. Tagami, M. Tsukada, H. Fukuyama, Phys. Rev. Lett. 94 (2005) 226403.
[34] T.O. Wehling, H.P. Dahal, A.I. Lichtenstein, A.V. Balatsky, Phys. Rev. B 78 (2008) 035414.
[35] D.-H. Lin, Phys. Rev. A 73 (2006) 044701.
[36] V.M. Pereira, F. Guinea, J.M.B.L. dos Santos, N.M.R. Peres, A.H.C. Neto, Phys. Rev. Lett. 96 (2006) 036801.
[37] A.C. Hewson, The Kondo Problem to Heavy Fermions, Cambridge University Press, 1993.
[38] M.I. Katsnelson, K.S. Novoselov, A.K. Geim, Nat. Phys. 2 (2006) 620.
[39] T. Ohta, A. Bostwick, T. Seyller, K. Horn, E. Rotenberg, Science 313 (2006) 951.
[40] S.Y. Zhou, D.A. Siegel, A.V. Fedorov, A. Lanzara, Phys. Rev. Lett. 101 (2008) 086402.
[41] J.H. Chen, C. Jang, S. Adam, M.S. Fuhrer, E.D. Williams, M. Ishigami, Nat. Phys. 4 (2008) 377.
[42] D.C. Elias et al., Science 323 (2009) 610.
[43] K.T. Chan, J.B. Neaton, M.L. Cohen, Phys. Rev. B 77 (2008) 235430.
[44] T.O. Wehling, M.I. Katsnelson, A.I. Lichtenstein, Monovalent impurities on graphene: midgap states and migration barriers, 2009 (unpublished). Available from: <arXiv:0903.2006>.
[45] M.I. Katsnelson, F. Guinea, A.K. Geim, Phys. Rev. B 79 (2009) 195426.
[46] J.C. Meyer, C.O. Girit, M.F. Crommie, A. Zettl, Nature 454 (2008) 319.
[47] D.W. Boukhvalov, M.I. Katsnelson, A.I. Lichtenstein, Phys. Rev. B 77 (2008) 035427.
[48] S. Casolo, O.M. Løvvik, R. Martinazzo, G.F. Tantardini, J. Chem. Phys. 130 (2009) 054704.
[49] J.P. Robinson, H. Schomerus, L. Oroszlány, V.I. Fal'ko, Phys. Rev. Lett. 101 (2008) 196803.
[50] O. Leenaerts, B. Partoens, F.M. Peeters, Phys. Rev. B 77 (2008) 125416.
[51] R.M. Ribeiro, N.M.R. Peres, J. Coutinho, P.R. Briddon, Phys. Rev. B 78 (2008) 075442.
[52] S. Meng, E. Kaxiras, Z. Zhang, J. Chem. Phys. 127 (2007) 244710.
[53] J.D. Bernal, R.H. Fowler, J. Chem. Phys. 1 (1933) 515.
[54] T.O. Wehling, A.I. Lichtenstein, M.I. Katsnelson, Appl. Phys. Lett. 93 (2008) 202110.
[55] J. Moser, A. Verdaguer, D. Jimenez, A. Barreiro, A. Bachtold, Appl. Phys. Lett. 92 (2008) 123507.
[56] M. Wilson, T.R. Walsh, J. Chem. Phys. 113 (2000) 9180.
[57] W. Kim, A. Javey, O. Vermesh, Q. Wang, Y. Li, H. Dai, Nano Lett. 3 (2003) 193.
[58] J. Martin, N. Akerman, G. Ulbricht, T. Lohmann, J.H. Smet, K. von Klitzing, A. Yacoby, Nat. Phys. 4 (2008) 144.
[59] A. Deshpande, W. Bao, F. Miao, C.N. Lau, B.J. LeRoy, Spatially resolved spectroscopy of monolayer graphene on SiO_2, 2008. Available from: <arXiv:0812.1073>.
[60] J.T. Robinson, F.K. Perkins, E.S. Snow, Z. Wei, P.E. Sheehan, Nano Lett. 8 (2008) 3137.

Tim Wehling studied physics in Göttingen and Hamburg (Germany) and received his diploma in physics at the University of Hamburg in 2006. Since then he has been working as a graduate student in the 1st Institute for Theoretical Physics at the University of Hamburg with continuous research stays at Los Alamos National Laboratory (USA).
His research is in the field of theoretical solid state physics with focus on the electronic properties of graphene and correlated nanoscale systems. He is a recipient of the Otto Stern Award (2006) of the University of Hamburg for his diploma research.

Mikhail Katsnelson received his PhD in solid state physics in 1980 from the Institute of Metal Physics (Ekaterinburg, Russia) where he stayed till 2001 (last position – head of the group of quantum theory of metals). From 1992, he was simultaneously a professor of solid state physics and of mathematical physics in Ural State University. After three years in Uppsala University, 2002–2004, as a visiting professor of theoretical magnetism, M. Katsnelson became professor and head of the group of theory of condensed matter in Radboud University Nijmegen. His main scientific interests cover quantum many-body theory, electronic structure and lattice properties of metals and alloys, and, especially, magnetism. Starting from discovery of graphene in 2004, his main activity is focused in this new field, combining theoretical support of experimental research, traditional 'pen-and-paper' theoretical physics, and computational material science and theoretical chemistry of graphene. He has been awarded the State Prize for young scientists of Russia (1988).

Alexander Lichtenstein received his PhD in theoretical physics in 1982 from the Institute of Solid State Chemistry (Ekaterinburg, Russia) where he stayed until 1988. From 1989 until 1997, he was staff member at the Max-Planck Institute for Solid State Physics in Stuttgart and at Forschungszentrum Jülich. From 1998 until 2004 he was a head of the computational material science group in Radboud University Nijmegen and since 2004 he is professor at the University of Hamburg.
His main scientific interests are related with the theory of magnetism and electronic correlations using combinations of first-principle density functional theory with many-body techniques. His awards include the Intel/RUSNANO High Performance Computing Prize (2008), the State Prize of Russia in science and technology (1995), and the State Prize for young scientists of Russia (1988).